



**University of
Zurich**^{UZH}

**Zurich Open Repository and
Archive**

University of Zurich
Main Library
Strickhofstrasse 39
CH-8057 Zurich
www.zora.uzh.ch

Year: 2016

The cerebellar mossy fiber synapse as a model for high-frequency transmission in the mammalian CNS

Delvendahl, Igor; Hallermann, Stefan

Abstract: The speed of neuronal information processing depends on neuronal firing frequency. Here, we describe the evolutionary advantages and ubiquitous occurrence of high-frequency firing within the mammalian nervous system in general. The highest firing frequencies so far have been observed at the cerebellar mossy fiber to granule cell synapse. The mechanisms enabling high-frequency transmission at this synapse are reviewed and compared with other synapses. Finally, information coding of high-frequency signals at the mossy fiber synapse is discussed. The exceptionally high firing frequencies and amenability to high-resolution technical approaches both in vitro and in vivo establish the cerebellar mossy fiber synapse as an attractive model to investigate high-frequency signaling from the molecular up to the network level.

DOI: <https://doi.org/10.1016/j.tins.2016.09.006>

Posted at the Zurich Open Repository and Archive, University of Zurich

ZORA URL: <https://doi.org/10.5167/uzh-134924>

Journal Article

Accepted Version



The following work is licensed under a Creative Commons: Attribution-NonCommercial-NoDerivatives 4.0 International (CC BY-NC-ND 4.0) License.

Originally published at:

Delvendahl, Igor; Hallermann, Stefan (2016). The cerebellar mossy fiber synapse as a model for high-frequency transmission in the mammalian CNS. *Trends in Neurosciences*, 39(11):722-737.

DOI: <https://doi.org/10.1016/j.tins.2016.09.006>

1 **Title: The cerebellar mossy fiber synapse as a model for high-**
2 **frequency transmission in the mammalian CNS**

3

4 **Authors:** Igor Delvendahl^{1,2} and Stefan Hallermann^{1,*}

5 **Affiliation:** ¹ Carl-Ludwig-Institute for Physiology, Medical Faculty, University of
6 Leipzig, Liebigstr. 27, 04103 Leipzig, Germany.

7 ² Present address: Institute for Molecular Life Sciences, University of Zurich,
8 Winterthurerstrasse 190, 8057 Zurich, Switzerland.

9 * Correspondence: hallermann@medizin.uni-leipzig.de

10

11 **Short title:** High-frequency synaptic transmission

12 **Keywords:** Synapse; Synaptic transmission; Cerebellum; High-frequency signaling

13

14 **Abstract**

15 The speed of neuronal information processing depends on neuronal firing frequency.
16 Here, we describe the evolutionary advantages and ubiquitous occurrence of high-
17 frequency firing within the mammalian nervous system in general. The highest firing
18 frequencies so far have been observed at the cerebellar mossy fiber to granule cell
19 KILL (GC) synapse. The mechanisms enabling high-frequency transmission at this
20 synapse are reviewed and compared with other synapses. Finally, information coding
21 of high-frequency signals at the mossy fiber synapse is discussed. The exceptionally
22 high firing frequencies and amenability to high-resolution technical approaches both
23 *in vitro* and *in vivo* establish the cerebellar mossy fiber synapse as an attractive
24 model to investigate high-frequency signaling from the molecular up to the network
25 level.

26

27 **Advantages and disadvantages of high-frequency rate coding**

28 The capacity for rapid information processing in the mammalian nervous system has
29 been optimized by natural selection. As a consequence, processing of, e.g., sensory
30 afferents from whiskers [1] or the cochlea [2] features a temporal precision in the
31 microsecond range in response to specific stimuli. A variety of neuronal mechanisms
32 evolved to process information rapidly. Here, we focus on the amazing ability of
33 neurons to fire trains of action potentials (APs) and transmit information at high
34 frequency (defined as frequencies well above 100 Hz). Other mechanisms, such as a
35 rapid axonal AP conduction and short synaptic delay, are also essential for rapid
36 information processing but will not be addressed in detail. We argue that high-
37 frequency transmission has evolutionary advantages (Figure 1) and occurs
38 ubiquitously in the mammalian central nervous system (CNS, Figure 2). We further
39 suggest that the cerebellar mossy fiber bouton (cMFB) to granule cell (GC) synapse
40 is an ideal model to analyze high-frequency signaling. The mechanisms underlying
41 high-frequency transmission are discussed and compared with other synapses
42 (Figures 3 and 4; Box 1). Finally, the function of high-frequency information coding *in*
43 *vivo* at the cMFB-GC synapse are discussed (Figure 5). Note that this argumentation
44 does not conflict with the fact that information processing occurs on a variety of time
45 scales and that many neurons of the CNS are optimized for efficient processing of
46 slow signals.

47

48 *The role of firing frequency for neuronal information processing*

49 In principle, a single neuron can encode information as the average firing rate
50 (referred to as **rate coding** (see Glossary)) and/or as the exact timing of spikes in a
51 pulse train (i.e. the temporal sequence, referred to as **temporal coding**). On the
52 level of a population of neurons, information may be encoded using rate code (that is,

53 average asynchronous firing rate across all neurons) or temporal code, but also via a
54 correlation code, rank-order code, and/or spatiotemporal pattern code (reviewed by
55 refs. [3, 4]). It is well established that sensory information as well as motor
56 commands are predominantly encoded via rate coding. In the CNS, as sensory
57 information is processed at successive stages, average firing frequencies tend to
58 decrease and temporal- and sparse coding become increasingly important [5] (Figure
59 1A). There is a debate as to which of these coding regimes dominates in the cerebral
60 cortex, which is beyond the scope of this article (but see, e.g., refs. [5, 6]).
61 Nevertheless, rate coding is an important possibility to encode information by
62 neurons. The temporal precision of a neuronal population employing rate coding is
63 determined by both the number of neurons and the maximal firing frequency of each
64 neuron [4]. Evolutionary constraints likely define the optimal firing frequency of
65 neurons; we argue that several such constraints favor the use of fewer neurons with
66 higher firing frequency. To illustrate this, let us look at a simple example of a
67 neuronal population consisting of two neurons each with 10 Hz average firing
68 frequency (Figure 1B). Alternatively, four neurons with 5 Hz firing frequency (left) or a
69 single neuron with 20 Hz firing frequency (right) will result in the same AP frequency
70 of the ensemble (20 Hz). What are the advantages and disadvantages of these
71 scenarios?

72

73 *Advantages of higher firing frequency and fewer neurons*

74 A smaller number of high-frequency firing neurons has the advantage of ultimately
75 leading to a smaller CNS with shorter conduction delays. In addition, the CNS will
76 have a lower weight, requiring less energy to carry it. Finally, less energy is required
77 to maintain cell biological function of the smaller number of neurons (energetic costs
78 for house-keeping and resting membrane potential of each neuron; ref. [7]).

79 However, high-frequency firing also has the following disadvantages: In general, the
80 metabolic efficiency of APs [8] seems to decrease with increasing firing frequency [9,
81 10]. Yet, APs at cMFBs, which can fire at >1 kHz frequency, are surprisingly efficient
82 (Na^+ excess ratio of only 1.8; ref. [11]). This is currently not well understood, but
83 argues against a biophysical requirement that metabolic efficiency decreases
84 strongly with increasing firing frequency. Another potential disadvantage of high firing
85 frequencies lies in the limited frequency response of synapses, which leads to a low-
86 pass filtering of neuronal signals. Yet, some synapses can transmit exceptionally
87 high-frequency signals (see below).

88
89 Thus, while there are strong evolutionary constraints arguing for a small number of
90 neurons, each operating at high firing frequency, the disadvantages of high-
91 frequency signaling are less obvious. Furthermore, some synapses, such as the
92 cMFB-GC synapse, seem to have largely reduced these disadvantages. It should be
93 noted, however, that less robust signaling with weak synaptic connections and
94 recurrent excitation might benefit from a large number of neurons with low firing
95 frequency as has been described in the cerebral cortex [6]. The major advantages of
96 fewer, high-frequency neurons are the reduced brain size and lower basal energy
97 consumption [7]. Energetic constraints thus argue for the use of high-frequency AP
98 firing and synaptic transmission. Note, that the maximum firing frequency of neurons
99 (1–2 kHz) is still more than six orders of magnitude slower compared with the clock
100 rate of modern computers [12]. The immense effort to further increase the clock rate
101 of computers is consistent with our argumentation. Taking into account the complex
102 interplay of proteins required for AP generation and synaptic transmission,
103 biophysical and energetic constraints might restrict the maximum signaling frequency
104 of neurons. Indeed, it has previously been argued that the brain's information

105 processing rate may be limited to a millisecond timescale by its energy supply [13]. In
106 summary, several arguments indicate advantages of neuronal high-frequency firing.
107 But to what extent does high-frequency signaling occur in the CNS?

108

109 **Occurrence of high-frequency signaling in the mammalian CNS**

110 Indeed, high-frequency firing occurs ubiquitously throughout the mammalian CNS. In
111 the cerebral cortex, subtypes of pyramidal neurons in layers 2/3 or layer 5 show a
112 typical burst firing behavior. Within such bursts, the frequency of APs can reach up to
113 300 Hz. So-called *fast rhythmic bursting* or *chattering* cells may even display
114 intraburst frequencies of ~800 Hz *in vivo* (ref. [14]; Figure 2A). Pyramidal neurons
115 have, however, a low average firing rate of just a few Hz. A subtype of GABAergic
116 interneurons in the cortex—fast-spiking parvalbumin-positive cells—provide
117 feedforward inhibition as well as feedback inhibition to principal cells and are, e.g.,
118 required for network oscillations [15]. These fast-spiking interneurons can sustain AP
119 firing at up to 500 Hz (ref. [16]; Figure 2B). Even higher AP frequencies have been
120 observed in axons and neurons along sensory pathways. In the auditory brainstem,
121 the localization of a sound source is achieved by processing of converging inputs
122 from both cochleae with microsecond precision [17]. This information is first
123 transmitted onto postsynaptic cells via large synaptic terminals, the calyces of Held.
124 In these presynaptic terminals, spiking and synaptic transmission at up to ~1 kHz
125 could be observed (ref. [18, 19]; Figure 2C). Also in the auditory pathway, neurons in
126 the medial superior olive and the ventral cochlear nucleus are capable of firing APs
127 at up to 1 kHz [20, 21]. Finally, cerebellar mossy fiber boutons (cMFBs), which
128 convey sensory information of different origin to the cerebellar cortex, exhibit
129 remarkably high AP frequencies. *In vivo*, AP frequencies of several hundreds of Hz
130 were measured upon sensory stimulation, reaching instantaneous frequencies of up

131 to 1 kHz and average frequencies of ~350 Hz during short bursts [22, 23]. *In vitro*,
132 APs can be reliably elicited at up to 1.6 kHz (ref. [11]; Figure 2D). To our knowledge,
133 these AP frequencies represent the highest values in neurons reported thus far.
134 However, it should be noted that the average firing frequencies of these example
135 neurons are generally much slower than the here reported maximum firing
136 frequencies.

137

138 All the above examples were collected in rodent models, but high-frequency neuronal
139 signaling is not limited to rodents. Indeed, there are indications for high-frequency
140 signaling in non-human primates, where high-frequency responses of ~600 Hz were
141 observed in response to stimulation of cerebellar output neurons using functional
142 magnetic resonance imaging [24]. In the human brain, oscillations of up to at least
143 600 Hz can be resolved in EEG recordings [25]. Furthermore, high-frequency
144 signaling occurs across numerous healthy and pathological brain states. For
145 example, it has been shown that high-frequency firing of thalamic neurons (up to
146 450 Hz) controls sleep [26] and that firing in the gamma-frequency (i.e., 25–100 Hz)
147 may play a role in some neuropsychiatric diseases [27]. On the other hand, high-
148 frequency firing has also been observed in invertebrates. Sensory touch detector
149 cells of spiders, for instance, can fire at 600 Hz upon mechanical stimulation [28].
150 These examples indicate that AP firing and synaptic transmission at high frequency
151 are fundamental for the function of the CNS in humans and throughout the animal
152 kingdom, making the understanding of high-frequency transmission an important goal
153 in neuroscience. In the following, we argue that the cMFB-GC synapse in rodents is
154 an ideal model to study the mechanisms and role of high-frequency transmission in
155 the CNS.

156

157

158 **The cMFB-GC synapse as a model for high-frequency transmission**

159 ***Structure of the cMFB-GC synapse***

160 Mossy fibers are myelinated axons originating from cells in, e.g., spinal cord, pontine
161 nuclei, vestibular nuclei, or cerebellar nuclei. They send collaterals to the deep
162 cerebellar nuclei [29] and enter the GC layer of the cerebellar cortex [30], where they
163 form several varicosities. These cMFBs have a complex shape with high surface-to-
164 volume ratio and a relatively large diameter of 3–12 μm [31]. Ultrastructural analyses
165 revealed that cMFBs contain a very large number of synaptic vesicles (~200,000; ref.
166 [31]) and many **active zones** (150–300; Table I in Box 1; refs. [32, 33]).

167

168 In the **cerebellar glomeruli**, a single cMFB makes *en passant* excitatory synaptic
169 contact with the dendrites of several cerebellar GCs. GCs have a small soma with 5–
170 7 μm diameter and on average only four short dendrites [34–36]. The dendrites rarely
171 exceed 20 μm in length and have a very thin diameter of ~0.6 μm [34–36]. Each GC
172 dendrite ends in claw-shaped digits surrounding a single cMFB [37]. Estimates of the
173 number of postsynaptic GCs per cMFB are in the range of 10–100 [11, 38], reflecting
174 a high degree of synaptic divergence. Thus, the cMFB-GC synapse is a highly
175 divergent synapse, structurally specialized to transmit information to many
176 postsynaptic neurons.

177

178

179 ***Techniques for examining the cMFB-GC synapse***

180 Patch-clamp recordings from the postsynaptic cerebellar GCs of mice *in situ* were
181 already performed in the early 1990s [34, 39], demonstrating that low-noise and high-
182 resolution synaptic currents could be resolved. Recently, whole-cell patch-clamp

183 recordings from dendrites of GCs were reported [35], which support the previously
184 estimated electrical compactness of GCs [34, 39].

185

186 Extracellular focal recordings from presynaptic cMFBs in mice allowed measurement
187 of changes in presynaptic currents during long-term potentiation [40]. Recently, direct
188 presynaptic patch-clamp recordings from cMFBs in rats [22], turtles [41], and mice
189 [11, 42-44] have extended the experimental possibilities at this synapse. Presynaptic
190 recordings from cMFBs offer excellent voltage-clamp conditions and can be paired
191 with recordings from postsynaptic GCs [11, 42]. Such recordings are also possible in
192 mature animals.

193

194 Furthermore, cMFBs offer the chance to perform direct presynaptic patch-clamp
195 recordings in anaesthetized [22] or behaving mammals (ref. [45]; cf. Table I). In
196 addition, GCs can be recorded from *in vivo* [45, 46]. The opportunity to combine high-
197 resolution biophysical techniques *in vitro* with direct recordings *in vivo* from both pre-
198 and postsynaptic compartments thus makes the cMFB-GC synapse ideally suited to
199 study neuronal high-frequency signaling.

200

201

202 **Presynaptic mechanisms enabling high-frequency synaptic transmission**

203 Using the above described high-resolution techniques, reliable synaptic transmission
204 at a frequency of 1 kHz has been described at the cMFB-GC synapse (ref. [11],
205 Figure 4A). In the following, we will review the specializations that seem essential for
206 synaptic information transmission at such high rates and compare these mechanisms
207 with other synapses that operate at high and low frequencies (Table I). We will

208 restrict our discussion on excitatory transmission (for inhibitory synapses see, e.g.,
209 refs. [47-50]) and focus on 11 points, which are illustrated in Figure 3.

210

211 ***(1) Short duration of the presynaptic AP***

212 The presynaptic APs in cMFBs have a duration at half-maximal amplitude of ~100 μ s
213 (ref. [11], Figure 4C). To our knowledge, this duration is the shortest reported thus
214 far, but such rapid APs are probably not a unique feature of cMFBs within the
215 mammalian CNS (see Table I). However, AP duration inversely correlates with
216 maximum firing frequency within a population of neurons (e.g. in cMFBs [11] and in
217 neurons of the vestibular nucleus [51]), and across types of neurons [52].

218

219 ***(2) Fast kinetics of presynaptic ion channels***

220 The Na⁺ and K⁺ currents underlying the AP have short half-durations of 73 μ s and
221 61 μ s, respectively (Figure 4C), and provide a surprising metabolic efficiency of the
222 AP (see Table I). The AP-evoked K⁺ current is mediated by voltage-gated K⁺
223 channels of the K_v1 and K_v3 subtypes [11]. Compared with other presynaptic
224 terminals, the contribution of the slower gating K_v1 channels [53] to the repolarization
225 of the rapid APs at cMFBs is surprising. It is currently also unclear if the K⁺ currents
226 at cMFBs show activity-dependent facilitation to support high-frequency firing as
227 described at the calyx of Held [54]. Despite the brevity of the APs at cMFBs,
228 presynaptic Ca²⁺ channels—predominantly of the Cav2.1 subtype—are effectively
229 opened during an AP [11].

230

231 ***(3) Low capacity of endogenous Ca²⁺ buffering***

232 In general, Ca²⁺ ions entering a presynaptic terminal during an AP are rapidly bound
233 by **endogenous Ca²⁺ buffers**. The binding capacity of fixed Ca²⁺ buffers at cMFBs is

234 very low (~15), leading to a rapid clearance of Ca^{2+} from the active zone (Figure 4C),
235 which explains the very synchronous release of synaptic vesicles [43]. The Ca^{2+}
236 binding capacity of endogenous buffers is similar at hippocampal mossy fiber
237 boutons and the calyx of Held (~20 and ~45, respectively; refs. [55, 56]), but higher
238 (~140) in boutons of cortical pyramidal neurons [57] (cf. Table I). In addition, a mobile
239 Ca^{2+} buffer with kinetics similar to EGTA supports high-frequency firing in cMFBs by
240 reducing the build-up of Ca^{2+} in between consecutive APs [43]. The properties of the
241 mobile buffer at cMFBs are comparable to that at the calyx of Held synapse [58].

242

243 **(4) Tight Ca^{2+} channel to vesicle coupling**

244 The coupling distance between synaptic vesicles and Ca^{2+} channels [59, 60] is
245 estimated to be ~20 nm at the cMFB-GC synapse (ref. [43], Figure 3). This tight
246 **nanodomain** coupling supports a very rapid time course of release [61]. A similar
247 coupling distance was estimated for the calyx of Held synapse [62, 63] and at parallel
248 fiber to Purkinje cell synapses [64] (see also refs. in [60]). In contrast, hippocampal
249 mossy fiber boutons, which operate at lower firing frequencies, exhibit a looser
250 coupling in the range of 75 nm [65]. And the coupling distance is even larger in
251 boutons of cortical or hippocampal pyramidal neurons (refs. [66, 67], Table I).

252

253 **(5) A large pool of synaptic vesicles with fast recruitment**

254 Initial recordings from GCs indicated that the readily releasable pool (**RRP**) for a
255 cMFB-GC connection consists of 5–10 vesicles, and that each vesicle in the RRP is
256 replenished from a pool of ~300 releasable vesicles with a high rate constant of 60–
257 80 s^{-1} (refs. [68-70], Table I). Direct presynaptic depolarizations of cMFBs revealed a
258 slightly larger RRP consisting of two populations of vesicles (~10 vesicles each) with
259 a slightly lower rate constant of vesicle recruitment (30 s^{-1} ; ref. [11]). Consistent with

260 these findings, a fast and slow releasing pool of vesicles has been measured at the
261 calyx of Held synapse using presynaptic depolarization (FRP and SRP, respectively,
262 ref. [71]), and AP-evoked release is mainly mediated by the FRP at this synapse [72].
263 In Table I of Box 1 we therefore differentiate between **RRP_{AP}** (corresponding to the
264 FRP at the calyx) and **RRP_{Depol}** (corresponding to FRP+SRP at the calyx). Note, that
265 the two pools of vesicles previously described at cMFBs [69] using AP-stimulation
266 (i.e. within RRP_{AP}) might correspond to different degrees of **superpriming** of FRP
267 vesicles at the calyx [73]. Finally, the high rate constant of vesicle replenishment is
268 consistent with recent experimentally constrained modeling results on rapid diffusion
269 of vesicles within cMFBs [74].

270

271 **(6) Very rapid endocytosis**

272 Following fusion of synaptic vesicles, the added presynaptic plasma membrane is
273 retrieved via endocytosis. There is a considerable controversy on the speed of this
274 process [75] and there are indications for different recycling mechanisms for
275 membranes and vesicle proteins [151]. Endocytosis is very fast (time constant <1 s)
276 in cultured neurons at physiological temperature [76] and room temperature [77], as
277 well as in salamander cone photoreceptors at room temperature [78]. At the calyx of
278 Held synapse, very fast endocytosis was observed at room temperature using
279 membrane capacitance measurements, too [79]. But it is unclear how much this
280 finding was influenced by artifacts [80]. The cMFB allows time-resolved high-
281 resolution capacitance measurements at 37 °C, which revealed a rapid time constant
282 of endocytosis following a single AP stimulus (~500 ms; ref. [42]; Figure 4B).

283

284 **Postsynaptic mechanisms enabling high-frequency synaptic transmission**

285 In addition to the presynaptic mechanisms above, sustained high-frequency
286 transmission at the cMFB-GC synapse is supported by several specializations of the
287 postsynaptic GCs.

288

289 ***(7) Rapid excitatory postsynaptic currents***

290 The excitatory postsynaptic currents (EPSCs) recorded from GCs have very rapid
291 rise and decay kinetics (ref. [34]; Figure 4C). GC EPSCs are predominantly mediated
292 by AMPA receptors composed of GluA2 and GluA4 subunits [37], similar to the calyx
293 of Held synapse [81]. In neocortical pyramidal neurons, on the other hand, GluA1 is
294 the dominant subunit, leading to slower kinetics of AMPA mediated currents [81]. In
295 addition, there is a contribution of NMDA receptors at the cMFB-GC synapse [34,
296 39], which supports synaptic transmission at high frequencies in mature synapses
297 [82, 83].

298

299 ***(8) Fast recovery from glutamate receptor desensitization***

300 The glutamate receptors in GCs enter slowly into desensitization states and have a
301 fast recovery from desensitization [84]. This relative resistance to AMPA receptor
302 desensitization supports high-frequency transmission, during which glutamate
303 accumulates in the synaptic cleft.

304

305 ***(9) Glutamate spillover from neighboring release sites***

306 Furthermore, there is a slow-rising component of AMPA-mediated EPSCs at the
307 cMFB-GC synapse caused by glutamate spillover from neighboring active zones (ref.
308 [85]; Figure 3). Spillover also contributes to the tonic component of the EPSC during
309 frequency-dependent short-term depression [68]. This tonic component generates a

310 persistent depolarization mediated by both AMPA and NMDA receptors, which helps
311 to maintain a high firing rate of GCs [22, 45].

312

313 ***(10) Compact synaptic ultrastructure***

314 The cMFB-GC synapse has a compact ultrastructure with several small synaptic
315 contacts to each GC dendrite (Table I). During development, the complexity of the
316 glomerular structure increases [37, 86]. An increasing complexity has also been
317 observed at the calyx of Held synapse, where more finger-like extensions occur
318 during development [87].

319

320 ***(11) Electrotonic compactness of dendrites and soma***

321 The small soma size and short dendrite length make GCs electrotonically highly
322 compact with soma and dendrites behaving as a single electrical compartment [34,
323 88]. Consequently, excitatory postsynaptic potentials (EPSPs) are subject to very
324 little dendritic filtering [35]. The compact electrotonic properties of GCs thus allow for
325 highly efficient integration of synaptic input [89]. Interestingly, postsynaptic neurons
326 of the calyx of Held synapse are also very compact, which differs from other
327 synapses, where dendrites low-pass filter synaptic input (but see ref [90]).

328

329 Together, these pre- and postsynaptic specializations mediate the exceptionally rapid
330 and high-frequency synaptic transmission with high fidelity at the cMFB-GC synapse.
331 Several of these mechanistic findings are likely specific to high-frequency synapses,
332 whereas other synaptic parameters are similar across different synapses operating at
333 low- and high-frequency (see Box 1).

334

335 **High-frequency coding at the cMFB-GC synapse *in vivo***

336 What are the functional implications of the rapid and high-frequency synaptic
337 signaling that can take place at the cMFB-GC synapse? Earlier work using
338 extracellular recordings in monkeys or cats indicated that mossy fiber axons exploit
339 high-frequency rate coding of sensory variables, such as proprioceptive coding of a
340 joint angle or eye saccade metrics, with continuous firing rates reaching 100 Hz (ref.
341 [91, 92], Figure 5A). More recent *in vivo* recordings from GCs of anaesthetized mice
342 demonstrated that mossy fibers carrying vestibular information, such as rotational
343 velocity, use continuous rate coding, exhibiting a highly linear relationship between
344 velocity and charge transfer (ref. [93], Figure 5B). In contrast, mossy fibers conveying
345 rapid discrete sensory events, such as the sensory response to air puff stimulation,
346 show burst firing behavior with maximum instantaneous frequencies of about 1 kHz
347 (refs. [22, 23]; cf. Figure 2D), arguing for temporal coding. Furthermore, direct *in vivo*
348 patch-clamp recordings from cMFBs of awake mice during locomotion indicate that
349 some mossy fibers can shift from sparse activity to a dense rate code during
350 movement (ref. [45], Figure 5C). How this information is transmitted to GCs has also
351 been addressed by *in vivo* studies. GCs have a low spontaneous firing frequency of
352 0.5 Hz [46], but fire bursts of APs upon sensory stimulation with frequencies rarely
353 exceeding 500 Hz [22, 45, 46]. Thus, both mossy fibers and GCs exhibit high-
354 frequency firing *in vivo*, in particular during short bursts of activity.

355

356 The possibility of direct pre- and postsynaptic recordings *in vivo* makes the cMFB-GC
357 an ideal model to investigate the functional role of high-frequency coding. But the
358 exact coding at the cMFB-GC synapse is still poorly understood. Yet, from a network
359 perspective it is clear that the main function of the cMFB-GC synapse is to distribute
360 sensory and efferent copy information to GCs. The population of GCs is thought to
361 detect patterns in the mossy fiber input [94], resulting in a sparser higher dimensional

362 code in GCs compared with mossy fibers [38]. During this information transmission,
363 the temporal precision of the cMFB-GC synapse is essential to reliably detect rapid
364 signals within a certain time window [95], to adaptively filter [96, 97], and to precisely
365 match motor copy and sensory information [98]. In addition, the sequential firing of
366 nearby GCs [99] and the successive activation of different sets of GCs [100] might
367 underlie temporal processing in the cerebellar cortex [101]. Consistent with the role
368 of the cerebellum in timing [100, 101], not only the frequency but also the time of AP
369 firing in cMFBs and GCs seems essential. Independent of the diverse and partly
370 controversial function of the cerebellar cortex, the cMFB-GC synapse thus conveys
371 signals with remarkable bandwidth to the large number of GCs most likely using rate
372 and temporal coding.

373

374 **Concluding Remarks and Future Perspectives**

375 Neuronal high-frequency signaling is abundant throughout the mammalian CNS
376 (Figure 2). At the mature cMFB-GC synapse, direct pre- and postsynaptic patch-
377 clamp recordings are feasible with excellent temporal resolution. Based on such
378 recordings, the fastest signaling in the mammalian CNS has been described at the
379 this synapse. Several mechanistic specializations of the cMFB-GC synapse enable
380 precise and rapid synaptic transfer of information at very high rates (Figure 4 and
381 Box 1). These include ultrafast APs, low endogenous calcium buffering, coupling of
382 vesicles to calcium channels in the 20 nm range, rapid vesicle recruitment from a
383 large pool of releasable vesicles, ultrafast endocytosis, and rapid glutamate receptors
384 with fast recovery from desensitization. Furthermore, this synapse allows *in vivo*
385 recordings from pre- and postsynaptic neurons, which have revealed high-frequency
386 coding in both cMFBs and GCs (Figure 5). Thus, the cMFB-GC synapse has been

387 established as an attractive model to study high-frequency signaling and its
388 implications for neuronal information processing.

389

390 More research is required to improve our understanding of high-frequency synaptic
391 transmission (see Outstanding Questions). In this context, the use of, e.g., super-
392 resolution microscopy [102, 103] will allow investigation of the structural-functional
393 relationship of high-frequency synapses. To gain more insights into the molecular
394 mechanisms, techniques allowing genetic perturbations might be extended [30].
395 Finally, presynaptic recordings in behaving mice [45] offer the chance to further
396 analyze high-frequency coding during behavior.

397

398

399

400 **Acknowledgements**

401 We would like to thank Jens Eilers, Maarten H.P. Kole, Erwin Neher, and Laurens
402 Witter for helpful discussions and comments on a previous version of the manuscript.
403 S.H. received funding from the German Research Foundation (HA 6386/2-2 and 3-2).

404

405 **References**

- 406
407 1. Bale, M.R., *et al.* (2015) Microsecond-scale timing precision in rodent
408 trigeminal primary afferents. *J. Neurosci.* 35, 5935–5940
409 2. Wagner, H., *et al.* (2005) Microsecond precision of phase delay in the auditory
410 system of the barn owl. *J. Neurophysiol.* 94, 1655–1658
411 3. Kumar, A., *et al.* (2010) Spiking activity propagation in neuronal networks:
412 reconciling different perspectives on neural coding. *Nat. Rev. Neurosci.* 11,
413 615–627
414 4. Rieke, F., *et al.* (1997) *Spikes: Exploring the Neural Code*. The MIT Press
415 5. Wolfe, J., *et al.* (2010) Sparse and powerful cortical spikes. *Curr. Opin.*
416 *Neurobiol.* 20, 306–312
417 6. Tchumatchenko, T., *et al.* (2011) Ultrafast population encoding by cortical
418 neurons. *J. Neurosci.* 31, 12171–12179
419 7. Harris, J.J. and Attwell, D. (2012) The energetics of CNS white matter. *J.*
420 *Neurosci.* 32, 356–371
421 8. Alle, H., *et al.* (2009) Energy-efficient action potentials in hippocampal mossy
422 fibers. *Science* 325, 1405–1408
423 9. Carter, B.C. and Bean, B.P. (2011) Incomplete inactivation and rapid recovery
424 of voltage-dependent sodium channels during high-frequency firing in
425 cerebellar Purkinje neurons. *J. Neurophysiol.* 105, 860–871
426 10. Hallermann, S., *et al.* (2012) State and location dependence of action potential
427 metabolic cost in cortical pyramidal neurons. *Nat. Neurosci.* 15, 1007–1014
428 11. Ritzau-Jost, A., *et al.* (2014) Ultrafast action potentials mediate kilohertz
429 signaling at a central synapse. *Neuron* 84, 152–163
430 12. Nagarajan, N. and Stevens, C.F. (2008) How does the speed of thought
431 compare for brains and digital computers? *Curr. Biol.* 18, R756–R758
432 13. Attwell, D. and Gibb, A. (2005) Neuroenergetics and the kinetic design of
433 excitatory synapses. *Nat. Rev. Neurosci.* 6, 841–849
434 14. Gray, C.M. and McCormick, D.A. (1996) Chattering cells: superficial pyramidal
435 neurons contributing to the generation of synchronous oscillations in the visual
436 cortex. *Science* 274, 109–113
437 15. Hu, H., *et al.* (2014) Interneurons. Fast-spiking, parvalbumin⁺ GABAergic
438 interneurons: from cellular design to microcircuit function. *Science* 345,
439 1255–1263
440 16. Azouz, R., *et al.* (1997) Physiological properties of inhibitory interneurons in
441 cat striate cortex. *Cereb. Cortex* 7, 534–545
442 17. Trussell, L.O. (1999) Synaptic mechanisms for coding timing in auditory
443 neurons. *Annu. Rev. Physiol.* 61, 477–496
444 18. Kim, J.H., *et al.* (2013) Dysmyelination of auditory afferent axons increases
445 the jitter of action potential timing during high-frequency firing. *J. Neurosci.* 33,
446 9402–9407
447 19. Blosa, M., *et al.* (2015) The extracellular matrix molecule brevican is an
448 integral component of the machinery mediating fast synaptic transmission at
449 the calyx of Held. *J. Physiol.* 593, 4341–4360
450 20. Scott, L.L., *et al.* (2007) Weak action potential backpropagation is associated
451 with high-frequency axonal firing capability in principal neurons of the gerbil
452 medial superior olive. *J. Physiol.* 583, 647–661

- 453 21. Oertel, D., *et al.* (2000) Detection of synchrony in the activity of auditory nerve
454 fibers by octopus cells of the mammalian cochlear nucleus. *Proc. Natl. Acad.*
455 *Sci. USA* 97, 11773–11779
- 456 22. Rancz, E.A., *et al.* (2007) High-fidelity transmission of sensory information by
457 single cerebellar mossy fibre boutons. *Nature* 450, 1245–1248
- 458 23. Garwicz, M., *et al.* (1998) Cutaneous receptive fields and topography of mossy
459 fibres and climbing fibres projecting to cat cerebellar C3 zone. *J. Physiol.* 512,
460 277–293
- 461 24. Sultan, F., *et al.* (2012) Unravelling cerebellar pathways with high temporal
462 precision targeting motor and extensive sensory and parietal networks. *Nat.*
463 *Commun.* 3, 924
- 464 25. Ritter, P., *et al.* (2008) High-frequency (600 Hz) population spikes in human
465 EEG delineate thalamic and cortical fMRI activation sites. *NeuroImage* 42,
466 483–490
- 467 26. McCormick, D.A. and Bal, T. (1997) Sleep and arousal: thalamocortical
468 mechanisms. *Annu. Rev. Neurosci.* 20, 185–215
- 469 27. Sauer, J.F., *et al.* (2015) Impaired fast-spiking interneuron function in a
470 genetic mouse model of depression. *eLife* 4, e04979
- 471 28. Albert, J.T., *et al.* (2001) Arthropod touch reception: spider hair sensilla as
472 rapid touch detectors. *J. Comp. Physiol. A* 187, 303–312
- 473 29. Pugh, J.R. and Raman, I.M. (2006) Potentiation of mossy fiber EPSCs in the
474 cerebellar nuclei by NMDA receptor activation followed by postinhibitory
475 rebound current. *Neuron* 51, 113–123
- 476 30. Kalinovsky, A., *et al.* (2011) Development of axon-target specificity of ponto-
477 cerebellar afferents. *PLoS Biol.* 9, e1001013
- 478 31. Rollenhagen, A., *et al.* (2007) Structural determinants of transmission at large
479 hippocampal mossy fiber synapses. *J. Neurosci.* 27, 10434–10444
- 480 32. Kim, H.W., *et al.* (2013) Three-dimensional imaging of cerebellar mossy fiber
481 rosettes by ion-abrasion scanning electron microscopy. *Microsc. Microanal.* 19
482 Suppl 5, 172–177
- 483 33. Xu-Friedman, M.A. and Regehr, W.G. (2003) Ultrastructural contributions to
484 desensitization at cerebellar mossy fiber to granule cell synapses. *J. Neurosci.*
485 23, 2182–2192
- 486 34. Silver, R.A., *et al.* (1992) Rapid-time-course miniature and evoked excitatory
487 currents at cerebellar synapses in situ. *Nature* 355, 163–166
- 488 35. Delvendahl, I., *et al.* (2015) Dendritic patch-clamp recordings from cerebellar
489 granule cells demonstrate electrotonic compactness. *Front. Cell. Neurosci.* 9,
490 93
- 491 36. Cathala, L., *et al.* (2003) Maturation of EPSCs and intrinsic membrane
492 properties enhances precision at a cerebellar synapse. *J. Neurosci.* 23, 6074–
493 6085
- 494 37. Cathala, L., *et al.* (2005) Changes in synaptic structure underlie the
495 developmental speeding of AMPA receptor-mediated EPSCs. *Nat. Neurosci.*
496 8, 1310–1318
- 497 38. Billings, G., *et al.* (2014) Network structure within the cerebellar input layer
498 enables lossless sparse encoding. *Neuron* 83, 960–974
- 499 39. D'Angelo, E., *et al.* (1990) Dual-component NMDA receptor currents at a
500 single central synapse. *Nature* 346, 467–470
- 501 40. Maffei, A., *et al.* (2002) Presynaptic current changes at the mossy fiber-
502 granule cell synapse of cerebellum during LTP. *J. Neurophysiol.* 88, 627–638

- 503 41. Thomsen, L.B., *et al.* (2010) Presynaptic calcium signalling in cerebellar
504 mossy fibres. *Front. Neural Circuits* 4, 1
- 505 42. Delvendahl, I., *et al.* (2016) Fast, Temperature-Sensitive and Clathrin-
506 Independent Endocytosis at Central Synapses. *Neuron* 90, 492–498
- 507 43. Delvendahl, I., *et al.* (2015) Reduced endogenous Ca²⁺ buffering speeds
508 active zone Ca²⁺ signaling. *Proc. Natl. Acad. Sci. USA* 112, E3075–3084
- 509 44. Gao, Z., *et al.* (2016) Excitatory Cerebellar Nucleocortical Circuit Provides
510 Internal Amplification during Associative Conditioning. *Neuron* 89, 645–657
- 511 45. Powell, K., *et al.* (2015) Synaptic representation of locomotion in single
512 cerebellar granule cells. *eLife* 4, e07290
- 513 46. Chadderton, P., *et al.* (2004) Integration of quanta in cerebellar granule cells
514 during sensory processing. *Nature* 428, 856–860
- 515 47. Rowan, M.J., *et al.* (2016) Synapse-Level Determination of Action Potential
516 Duration by K⁺ Channel Clustering in Axons. *Neuron* 91, 370–383
- 517 48. Kawaguchi, S.Y. and Sakaba, T. (2015) Control of inhibitory synaptic outputs
518 by low excitability of axon terminals revealed by direct recording. *Neuron* 85,
519 1273–1288
- 520 49. Begum, R., *et al.* (2016) Action potential broadening in a presynaptic
521 channelopathy. *Nat. Commun.* 7, 12102
- 522 50. Hu, H. and Jonas, P. (2014) A supercritical density of Na⁺ channels ensures
523 fast signaling in GABAergic interneuron axons. *Nat. Neurosci.* 17, 686–693
- 524 51. Gittis, A.H., *et al.* (2010) Mechanisms of sustained high firing rates in two
525 classes of vestibular nucleus neurons: differential contributions of resurgent
526 Na, Kv3, and BK currents. *J. Neurophysiol.* 104, 1625–1634
- 527 52. Carter, B.C. and Bean, B.P. (2009) Sodium entry during action potentials of
528 mammalian neurons: incomplete inactivation and reduced metabolic efficiency
529 in fast-spiking neurons. *Neuron* 64, 898–909
- 530 53. Alle, H., *et al.* (2011) Sparse but highly efficient Kv3 outpace BKCa channels
531 in action potential repolarization at hippocampal mossy fiber boutons. *J.*
532 *Neurosci.* 31, 8001–8012
- 533 54. Yang, Y.M., *et al.* (2014) Enhancing the fidelity of neurotransmission by
534 activity-dependent facilitation of presynaptic potassium currents. *Nat.*
535 *Commun.* 5, 4564
- 536 55. Helmchen, F., *et al.* (1997) Calcium dynamics associated with a single action
537 potential in a CNS presynaptic terminal. *Biophys. J.* 72, 1458–1471
- 538 56. Jackson, M.B. and Redman, S.J. (2003) Calcium dynamics, buffering, and
539 buffer saturation in the boutons of dentate granule-cell axons in the hilus. *J.*
540 *Neurosci.* 23, 1612–1621
- 541 57. Koester, H.J. and Sakmann, B. (2000) Calcium dynamics associated with
542 action potentials in single nerve terminals of pyramidal cells in layer 2/3 of the
543 young rat neocortex. *J. Physiol.* 529, 625–646
- 544 58. Müller, M., *et al.* (2007) Parvalbumin is a mobile presynaptic Ca²⁺ buffer in the
545 calyx of held that accelerates the decay of Ca²⁺ and short-term facilitation. *J.*
546 *Neurosci.* 27, 2261–2271
- 547 59. Eggermann, E., *et al.* (2012) Nanodomain coupling between Ca²⁺ channels
548 and sensors of exocytosis at fast mammalian synapses. *Nat. Rev. Neurosci.*
549 13, 7–21
- 550 60. Stanley, E.F. (2016) The nanophysiology of fast transmitter release. *Trends*
551 *Neurosci.* 39, 183–197

- 552 61. Sargent, P.B., *et al.* (2005) Rapid vesicular release, quantal variability, and
553 spillover contribute to the precision and reliability of transmission at a
554 glomerular synapse. *J. Neurosci.* 25, 8173–8187
- 555 62. Wang, L.Y., *et al.* (2008) Synaptic vesicles in mature calyx of Held synapses
556 sense higher nanodomain calcium concentrations during action potential-
557 evoked glutamate release. *J. Neurosci.* 28, 14450–14458
- 558 63. Nakamura, Y., *et al.* (2015) Nanoscale Distribution of Presynaptic Ca²⁺
559 Channels and Its Impact on Vesicular Release during Development. *Neuron*
560 85, 145–158
- 561 64. Schmidt, H., *et al.* (2013) Nanodomain Coupling at an Excitatory Cortical
562 Synapse. *Curr. Biol.* 23, 244–249
- 563 65. Vyleta, N.P. and Jonas, P. (2014) Loose coupling between Ca²⁺ channels and
564 release sensors at a plastic hippocampal synapse. *Science* 343, 665–670
- 565 66. Rozov, A., *et al.* (2001) Transmitter release modulation by intracellular Ca²⁺
566 buffers in facilitating and depressing nerve terminals of pyramidal cells in layer
567 2/3 of the rat neocortex indicates a target cell-specific difference in presynaptic
568 calcium dynamics. *J. Physiol.* 531, 807–826
- 569 67. Ohana, O. and Sakmann, B. (1998) Transmitter release modulation in nerve
570 terminals of rat neocortical pyramidal cells by intracellular calcium buffers. *J.*
571 *Physiol.* 513, 135–148
- 572 68. Saviane, C. and Silver, R.A. (2006) Fast vesicle reloading and a large pool
573 sustain high bandwidth transmission at a central synapse. *Nature* 439, 983–
574 987
- 575 69. Hallermann, S., *et al.* (2010) Bassoon speeds vesicle reloading at a central
576 excitatory synapse. *Neuron* 68, 710–723
- 577 70. Hallermann, S. and Silver, R.A. (2013) Sustaining rapid vesicular release at
578 active zones: potential roles for vesicle tethering. *Trends Neurosci.* 36, 185–
579 194
- 580 71. Neher, E. and Sakaba, T. (2008) Multiple roles of calcium ions in the
581 regulation of neurotransmitter release. *Neuron* 59, 861–872
- 582 72. Sakaba, T. (2006) Roles of the fast-releasing and the slowly releasing vesicles
583 in synaptic transmission at the calyx of Held. *J. Neurosci.* 26, 5863–5871
- 584 73. Taschenberger, H., *et al.* (2016) Superpriming of synaptic vesicles as a
585 common basis for intersynapse variability and modulation of synaptic strength.
586 *Proc. Natl. Acad. Sci. USA* 113, E4548–4557
- 587 74. Rothman, J.S., *et al.* (2016) Physical determinants of vesicle mobility and
588 supply at a central synapse. *eLife* 5, in press (doi: 10.7554/eLife.15133)
- 589 75. Kononenko, N.L. and Haucke, V. (2015) Molecular mechanisms of presynaptic
590 membrane retrieval and synaptic vesicle reformation. *Neuron* 85, 484–496
- 591 76. Watanabe, S., *et al.* (2013) Ultrafast endocytosis at mouse hippocampal
592 synapses. *Nature* 504, 242–247
- 593 77. Leitz, J. and Kavalali, E.T. (2014) Fast retrieval and autonomous regulation of
594 single spontaneously recycling synaptic vesicles. *eLife* 3, e03658
- 595 78. Van Hook, M.J. and Thoreson, W.B. (2012) Rapid synaptic vesicle
596 endocytosis in cone photoreceptors of salamander retina. *J. Neurosci.* 32,
597 18112–18123
- 598 79. Sun, J.Y., *et al.* (2002) Single and multiple vesicle fusion induce different rates
599 of endocytosis at a central synapse. *Nature* 417, 555–559
- 600 80. Yamashita, T., *et al.* (2005) Vesicle endocytosis requires dynamin-dependent
601 GTP hydrolysis at a fast CNS synapse. *Science* 307, 124–127

- 602 81. Geiger, J.R., *et al.* (1995) Relative abundance of subunit mRNAs determines
603 gating and Ca²⁺ permeability of AMPA receptors in principal neurons and
604 interneurons in rat CNS. *Neuron* 15, 193–204
- 605 82. D'Angelo, E., *et al.* (1995) Synaptic excitation of individual rat cerebellar
606 granule cells in situ: evidence for the role of NMDA receptors. *J. Physiol.* 484,
607 397–413
- 608 83. Baade, C., *et al.* (2016) NMDA receptors amplify mossy fiber synaptic inputs
609 at frequencies up to at least 750 Hz in cerebellar granule cells. *Synapse* 70,
610 269–276
- 611 84. DiGregorio, D.A., *et al.* (2007) Desensitization properties of AMPA receptors
612 at the cerebellar mossy fiber granule cell synapse. *J. Neurosci.* 27, 8344–8357
- 613 85. DiGregorio, D.A., *et al.* (2002) Spillover of glutamate onto synaptic AMPA
614 receptors enhances fast transmission at a cerebellar synapse. *Neuron* 35,
615 521–533
- 616 86. Hámosi, J. and Somogyi, J. (1983) Differentiation of cerebellar mossy fiber
617 synapses in the rat: a quantitative electron microscope study. *J. Comp.*
618 *Neurol.* 220, 365–377
- 619 87. Taschenberger, H., *et al.* (2002) Optimizing synaptic architecture and
620 efficiency for high-frequency transmission. *Neuron* 36, 1127–1143
- 621 88. D'Angelo, E., *et al.* (1993) Different proportions of N-methyl-D-aspartate and
622 non-N-methyl-D-aspartate receptor currents at the mossy fibre-granule cell
623 synapse of developing rat cerebellum. *Neuroscience* 53, 121–130
- 624 89. London, M. and Häusser, M. (2005) Dendritic computation. *Annu. Rev.*
625 *Neurosci.* 28, 503–532
- 626 90. Golding, N.L. and Oertel, D. (2012) Synaptic integration in dendrites:
627 exceptional need for speed. *J. Physiol.* 590, 5563–5569
- 628 91. van Kan, P.L., *et al.* (1993) Movement-related inputs to intermediate
629 cerebellum of the monkey. *J. Neurophysiol.* 69, 74–94
- 630 92. Prsa, M., *et al.* (2009) Characteristics of responses of Golgi cells and mossy
631 fibers to eye saccades and saccadic adaptation recorded from the posterior
632 vermis of the cerebellum. *J. Neurosci.* 29, 250–262
- 633 93. Arenz, A., *et al.* (2008) The contribution of single synapses to sensory
634 representation in vivo. *Science* 321, 977–980
- 635 94. Marr, D. (1969) A theory of cerebellar cortex. *J. Physiol.* 202, 437–470
- 636 95. D'Angelo, E. and De Zeeuw, C.I. (2009) Timing and plasticity in the
637 cerebellum: focus on the granular layer. *Trends Neurosci.* 32, 30–40
- 638 96. Jörntell, H. and Ekerot, C.F. (2006) Properties of somatosensory synaptic
639 integration in cerebellar granule cells in vivo. *J. Neurosci.* 26, 11786–11797
- 640 97. Dean, P., *et al.* (2010) The cerebellar microcircuit as an adaptive filter:
641 experimental and computational evidence. *Nat. Rev. Neurosci.* 11, 30–43
- 642 98. Kennedy, A., *et al.* (2014) A temporal basis for predicting the sensory
643 consequences of motor commands in an electric fish. *Nat. Neurosci.* 17, 416–
644 422
- 645 99. Heck, D., *et al.* (2001) Sequential stimulation of rat cerebellar granular layer in
646 vivo: Further evidence of a 'tidal-wave' timing mechanism in the cerebellum.
647 *Neurocomputing* 38, 641–646
- 648 100. Medina, J.F., *et al.* (2000) Timing mechanisms in the cerebellum: testing
649 predictions of a large-scale computer simulation. *J. Neurosci.* 20, 5516–5525
- 650 101. Mauk, M.D. and Buonomano, D.V. (2004) The neural basis of temporal
651 processing. *Annu. Rev. Neurosci.* 27, 307–340

- 652 102. Ehmman, N., *et al.* (2014) Quantitative super-resolution imaging of Bruchpilot
653 distinguishes active zone states. *Nat. Commun.* 5, 4650
- 654 103. Nangneri, S., *et al.* (2012) Three-dimensional, tomographic super-resolution
655 fluorescence imaging of serially sectioned thick samples. *PloS one* 7, e38098
- 656 104. Wang, S.S., *et al.* (2016) Fusion Competent Synaptic Vesicles Persist upon
657 Active Zone Disruption and Loss of Vesicle Docking. *Neuron* 91, 777-791
- 658 105. Neher, E. (2015) Merits and Limitations of Vesicle Pool Models in View of
659 Heterogeneous Populations of Synaptic Vesicles. *Neuron* 87, 1131-1142
- 660 106. Thanawala, M.S. and Regehr, W.G. (2013) Presynaptic calcium influx controls
661 neurotransmitter release in part by regulating the effective size of the readily
662 releasable pool. *J. Neurosci.* 33, 4625-4633
- 663 107. Pan, B. and Zucker, R.S. (2009) A general model of synaptic transmission and
664 short-term plasticity. *Neuron* 62, 539-554
- 665 108. Kole, M.H. (2011) First node of Ranvier facilitates high-frequency burst
666 encoding. *Neuron* 71, 671-682
- 667 109. de Kock, C.P. and Sakmann, B. (2008) High frequency action potential bursts
668 (≥ 100 Hz) in L2/3 and L5B thick tufted neurons in anaesthetized and
669 awake rat primary somatosensory cortex. *J. Physiol.* 586, 3353-3364
- 670 110. Renden, R. and von Gersdorff, H. (2007) Synaptic vesicle endocytosis at a
671 CNS nerve terminal: faster kinetics at physiological temperatures and
672 increased endocytotic capacity during maturation. *J. Neurophysiol.* 98, 3349-
673 3359
- 674 111. Molnár, G., *et al.* (2016) Human pyramidal to interneuron synapses are
675 mediated by multi-vesicular release and multiple docked vesicles. *eLife* 5,
676 e18167
- 677 112. Pernia-Andrade, A.J. and Jonas, P. (2014) Theta-gamma-modulated synaptic
678 currents in hippocampal granule cells in vivo define a mechanism for network
679 oscillations. *Neuron* 81, 140-152
- 680 113. Lisman, J. (1997) Bursts as a unit of neural information: making unreliable
681 synapses reliable. *Trends Neurosci.* 20, 38-43
- 682 114. Forsythe, I.D. (1994) Direct patch recording from identified presynaptic
683 terminals mediating glutamatergic EPSCs in the rat CNS, in vitro. *J. Physiol.*
684 479, 381-387
- 685 115. Geiger, J.R.P. and Jonas, P. (2000) Dynamic control of presynaptic Ca^{2+}
686 inflow by fast-inactivating K^+ channels in hippocampal mossy fiber boutons.
687 *Neuron* 28, 927-939
- 688 116. Jakab, R.L. and Hámosi, J. (1988) Quantitative morphology and synaptology
689 of cerebellar glomeruli in the rat. *Anat. Embryol.* 179, 81-88
- 690 117. Hoffpauir, B.K., *et al.* (2006) Synaptogenesis of the calyx of Held: rapid onset
691 of function and one-to-one morphological innervation. *J. Neurosci.* 26, 5511-
692 5523
- 693 118. Koester, H.J. and Johnston, D. (2005) Target cell-dependent normalization of
694 transmitter release at neocortical synapses. *Science* 308, 863-866
- 695 119. Holderith, N., *et al.* (2012) Release probability of hippocampal glutamatergic
696 terminals scales with the size of the active zone. *Nat. Neurosci.* 15, 988-997
- 697 120. Sätzler, K., *et al.* (2002) Three-dimensional reconstruction of a calyx of Held
698 and its postsynaptic principal neuron in the medial nucleus of the trapezoid
699 body. *J. Neurosci.* 22, 10567-10579
- 700 121. Silver, R.A., *et al.* (2003) High-probability unquantal transmission at excitatory
701 synapses in barrel cortex. *Science* 302, 1981-1984

- 702 122. Schikorski, T. and Stevens, C.F. (1997) Quantitative ultrastructural analysis of
703 hippocampal excitatory synapses. *J. Neurosci.* 17, 5858–5867
- 704 123. Taschenberger, H. and von Gersdorff, H. (2000) Fine-tuning an auditory
705 synapse for speed and fidelity: developmental changes in presynaptic
706 waveform, EPSC kinetics, and synaptic plasticity. *J. Neurosci.* 20, 9162–9173
- 707 124. Kole, M., *et al.* (2007) Axon initial segment Kv1 channels control axonal action
708 potential waveform and synaptic efficacy. *Neuron* 55, 633–647
- 709 125. Leão, R.M., *et al.* (2005) Presynaptic Na⁺ channels: locus, development, and
710 recovery from inactivation at a high-fidelity synapse. *J. Neurosci.* 25, 3724–
711 3738
- 712 126. Sola, E., *et al.* (2004) Increased neurotransmitter release during long-term
713 potentiation at mossy fibre-granule cell synapses in rat cerebellum. *J. Physiol.*
714 557, 843–861
- 715 127. Schneggenburger, R. and Neher, E. (2000) Intracellular calcium dependence
716 of transmitter release rates at a fast central synapse. *Nature* 406, 889–893
- 717 128. Hosoi, N., *et al.* (2007) Quantitative analysis of calcium-dependent vesicle
718 recruitment and its functional role at the calyx of Held synapse. *J. Neurosci.*
719 27, 14286–14298
- 720 129. Lawrence, J.J., *et al.* (2004) Quantal transmission at mossy fibre targets in the
721 CA3 region of the rat hippocampus. *J. Physiol.* 554, 175–193
- 722 130. Rosenmund, C., *et al.* (1993) Nonuniform Probability of Glutamate Release at
723 a Hippocampal Synapse. *Science* 262, 754–757
- 724 131. Branco, T., *et al.* (2008) Local Dendritic Activity Sets Release Probability at
725 Hippocampal Synapses. *Neuron* 59, 475–485
- 726 132. Nadkarni, S., *et al.* (2012) Short-term plasticity constrains spatial organization
727 of a hippocampal presynaptic terminal. *Proc. Natl. Acad. Sci. USA* 109,
728 14657–14662
- 729 133. Scimemi, A. and Diamond, J.S. (2012) The number and organization of Ca²⁺
730 channels in the active zone shapes neurotransmitter release from schaffer
731 collateral synapses. *J. Neurosci.* 32, 18157–18176
- 732 134. Schikorski, T. and Stevens, C.F. (2001) Morphological correlates of
733 functionally defined synaptic vesicle populations. *Nat. Neurosci.* 4, 391–395
- 734 135. Hallermann, S., *et al.* (2003) A large pool of releasable vesicles in a cortical
735 glutamatergic synapse. *Proc. Natl. Acad. Sci. USA* 100, 8975–8980
- 736 136. Kushmerick, C., *et al.* (2006) Physiological temperatures reduce the rate of
737 vesicle pool depletion and short-term depression via an acceleration of vesicle
738 recruitment. *J. Neurosci.* 26, 1366–1377
- 739 137. Neher, E. (2010) What is Rate-Limiting during Sustained Synaptic Activity:
740 Vesicle Supply or the Availability of Release Sites. *Front. Synaptic Neurosci.*
741 2, 144
- 742 138. Klyachko, V.A. and Stevens, C.F. (2006) Temperature-dependent shift of
743 balance among the components of short-term plasticity in hippocampal
744 synapses. *J. Neurosci.* 26, 6945–6957
- 745 139. Lin, K.H., *et al.* (2011) Presynaptic Ca²⁺ influx and vesicle exocytosis at the
746 mouse endbulb of Held: a comparison of two auditory nerve terminals. *J.*
747 *Physiol.* 589, 4301–4320
- 748 140. Han, Y.Y., *et al.* (2015) RIM1 and RIM2 redundantly determine Ca²⁺ channel
749 density and readily releasable pool size at a large hindbrain synapse. *J.*
750 *Neurophysiol.* 113, 255–263
- 751 141. Bischofberger, J., *et al.* (2002) Timing and efficacy of Ca²⁺ channel activation
752 in hippocampal mossy fiber boutons. *J. Neurosci.* 22, 10593–10602

- 753 142. Novak, P., *et al.* (2013) Nanoscale-targeted patch-clamp recordings of
754 functional presynaptic ion channels. *Neuron* 79, 1067–1077
- 755 143. Müller, A., *et al.* (2005) Endogenous Ca²⁺ buffer concentration and Ca²⁺
756 microdomains in hippocampal neurons. *J. Neurosci.* 25, 558–565
- 757 144. Shu, Y., *et al.* (2006) Modulation of intracortical synaptic potentials by
758 presynaptic somatic membrane potential. *Nature* 441, 761–765
- 759 145. Smith, S.M., *et al.* (2004) Recordings from single neocortical nerve terminals
760 reveal a nonselective cation channel activated by decreases in extracellular
761 calcium. *Neuron* 41, 243–256
- 762 146. Sasaki, T., *et al.* (2011) Action-potential modulation during axonal conduction.
763 *Science* 331, 599–601
- 764 147. Chabrol, F.P., *et al.* (2015) Synaptic diversity enables temporal coding of
765 coincident multisensory inputs in single neurons. *Nat. Neurosci.* 18, 718–727
- 766 148. Guzman, S.J., *et al.* (2016) Synaptic mechanisms of pattern completion in the
767 hippocampal CA3 network. *Science* 353, 1117–1123
- 768 149. Keller, D., *et al.* (2015) An Exclusion Zone for Ca²⁺ Channels around Docked
769 Vesicles Explains Release Control by Multiple Channels at a CNS Synapse.
770 *PLoS Comput. Biol.* 11, e1004253
- 771 150. Lee, J.S., *et al.* (2012) Actin-dependent rapid recruitment of reluctant synaptic
772 vesicles into a fast-releasing vesicle pool. *Proc. Natl. Acad. Sci. USA* 109,
773 E765–774
- 774 151. Okamoto, Y., *et al.* (2016) Distinct modes of endocytotic presynaptic
775 membrane and protein uptake at the calyx of Held terminal of rats and mice.
776 *eLife* 5, e14643
777

778 **Glossary**

779 **Active Zone:** refers to the specialized area of presynaptic plasma membrane and
780 the associated protein network where vesicle release occurs. Active zones thus
781 include presynaptic Ca^{2+} channels and several evolutionary conserved proteins that
782 are involved in docking and priming of synaptic vesicles, recruitment of Ca^{2+}
783 channels, and tethering of vesicles. Note that active zones are not required for fusion
784 competence of vesicles per se [104], but rather seem to increase release probability
785 and organize vesicle recruitment.

786 **Cerebellar glomerulus:** contains a single mossy fiber bouton or terminal that
787 contacts several granule cell dendrites and Golgi cell dendrites. In addition, a
788 cerebellar glomerulus typically also includes axons of inhibitory Golgi cells. The
789 glomerular structure is ensheathed by glia.

790 **Deconvolution technique:** can be used to estimate the time course of presynaptic
791 vesicle release by measuring the postsynaptic current. The current is deconvolved
792 using the measured waveform of miniature postsynaptic currents originating from
793 spontaneous single vesicle fusion and a calculated 'residual' current due to
794 glutamate accumulation in the synaptic cleft. For this type of deconvolution analysis,
795 paired recordings between presynaptic terminal and postsynaptic neuron are
796 required.

797 **Endogenous Ca^{2+} buffers:** these are proteins with Ca^{2+} binding domains that alter
798 the spatiotemporal characteristics of intracellular Ca^{2+} . Endogenous Ca^{2+} buffers can
799 be classified as fixed (immobile) or mobile. Typical proteins that constitute
800 endogenous mobile buffers include calretinin, parvalbumin, and calbindin, whereas
801 the identity of endogenous fixed Ca^{2+} buffers remains largely unknown.

802 **Nanodomain:** refers to a very localized presynaptic Ca^{2+} signal that governs release
803 of synaptic vesicles. Nanodomain coupling usually refers to vesicle-to- Ca^{2+} -channel

804 distances of <100 nm, with larger distances being termed microdomain. The vesicle-
805 to-Ca²⁺-channel may change during development, and many adult synapses rely on
806 nanodomain coupling.

807 **Rate coding:** can be used by neurons to represent information. For rate-coded
808 signaling, the frequency of APs within a certain time frame—and not the temporal
809 occurrence of APs—conveys the required information. Rate coding is typical in many
810 sensory systems and motoneurons.

811 **RRP:** The pool of readily releasable vesicles is heterogeneous [105, 106] and might
812 even be a “fussy concept” [107]. Here, we differentiate between the RRP that can be
813 evoked by APs (RRP_{AP}) and by depolarizations (RRP_{Depol}).

814 **RRP_{AP}:** is measured with, e.g., fluctuation analysis and back-extrapolations [105,
815 106], but postsynaptic receptor saturation can cause an underestimation of this RRP.

816 **RRP_{Depol}:** With depolarizations, an additional pool of slowly releasing vesicles (SRP;
817 ref. [71]) can be released, which is probably not being released by APs [72].

818 However, dissecting SRP and vesicle recruitment is difficult. In general, the higher
819 the rate of vesicle recruitment is assumed, the smaller the RRP will be. For example,
820 neglecting vesicle recruitment during depolarizations (with a duration of often
821 >30 ms) or sucrose application (often >1 s) can lead to an overestimation of the
822 RRP.

823 **Superpriming:** describes an additional increase in release probability of synaptic
824 vesicles after having been docked and primed at the presynaptic plasma membrane.

825 **Temporal coding:** refers to a type of information representation that relies on the
826 temporal correlation of APs in different neurons. Temporal coding can be used for
827 coincidence detection and plays an important role in oscillating neuronal networks.

828

829 **Trends Box**

- 830 • Recent studies using high-resolution methods revealed the remarkable speed
831 of synaptic transmission at central synapses.
- 832 • Very rapid release of presynaptic vesicles is supported by fast ion channels,
833 brief action potentials, fast vesicle recruitment, and tight nanodomain coupling.
- 834 • Fast kinetics of excitatory postsynaptic currents ensures rapid and efficient
835 integration.
- 836 • Mechanisms of high-frequency transmission may be similar between different
837 types of synapses.

838

839 **Outstanding Questions Box**

- 840 • In previous studies, the frequency of action potential firing and of synaptic
841 transmission may have been underestimated due to limited temporal
842 resolution (see Box 1). Are other synapses capable of similar high-frequency
843 signaling?
- 844 • Does the ability of a synapse to operate at high-frequency indicate that such
845 frequencies are used *in vivo*? Or in other words, did previous *in vivo* studies in
846 anaesthetized or head fixed animals underestimate the maximal firing
847 frequencies that could occur during, e.g., fight-and-flight reactions?
- 848 • What are the molecular mechanisms underlying high-frequency transmission?
849 Is this synaptic feature mediated by stoichiometry of the proteins or by
850 functional modifications of proteins such as phosphorylation?
- 851 • What are the ultrastructural specializations of synapses and active zones
852 enabling high-frequency synaptic transmission?
- 853 • What are the important cues locally to induce the formation of cMFBs
854 originating from various brain regions?
- 855 • How high are the metabolic costs of neuronal high-frequency signaling?
856

857 **Box 1: Tuning of synapses for high-frequency signaling**

858 To better understand how synapses are tuned for high-frequency signaling, we here
859 compare synaptic parameters of several excitatory synapses with gradually
860 decreasing instantaneous maximum firing frequencies *in vivo* (Table I): The cMFB-
861 GC and the calyx of Held synapse with very high frequency, neocortical pyramidal
862 cells with layer- and cell-type-specific intermediate frequency, and hippocampal
863 synapses with lower frequencies.

864

865 The high connectivity (Table I) of the cMFB is a unique feature among these
866 synapses. The number of active zones (Table I) varies among both high- and low-
867 frequency synapses. In contrast, the AP half-width (Table I) appears to be related to
868 maximum firing frequency. However, small errors in pipette capacitance
869 compensation can cause under- or overestimation of AP duration (and notably also
870 of the maximum firing frequency). The metabolic efficiency and the Ca^{2+} channel to
871 vesicle coupling distance (Table I) also seem to be linked to firing frequency. Thus,
872 high-frequency synapses tend to have rapid APs with rather low metabolic efficiency
873 [8, 10, 52] and exhibit tight Ca^{2+} channel to vesicle coupling [59, 60].

874 Regarding the remaining parameters, there is a striking lack of reliable quantitative
875 data. In particular, the fundamental parameter of the RRP per active zone is difficult
876 to define and measure [105]. To facilitate comparison, we differentiate between an
877 RRP that can be released by APs (RRP_{AP}) and an RRP that can be released by
878 presynaptic depolarizations ($\text{RRP}_{\text{Depol}}$; see Glossary for more information). Despite
879 the difficulty to accurately measure RRP and number of AZs, cMFBs seem to have
880 a uniquely small RRP_{AP} and $\text{RRP}_{\text{Depol}}$ per AZ, consistent with their small active zone
881 diameter (Table I) [70]. Furthermore, the high rate constant of vesicle replenishment
882 and the high release probability (Table I) seem specific for cMFBs and not

883 characteristic for high-frequency synapses. But there is still a surprising uncertainty in
884 the rate of vesicle recruitment, which seems related to the limited precision of the
885 RRP definition (see above; [70]). The Ca^{2+} -binding ratio (κ_E ; Table I) is often not
886 differentiated for fixed ($\kappa_{E,\text{fix}}$) and mobile buffers, which complicates a comparison.
887 Furthermore, estimates based on dye loading of boutons via the somatic patch
888 pipette can cause underestimation of $\kappa_{E,\text{fix}}$. Nevertheless, with the exception of $\kappa_{E,\text{fix}} =$
889 20 at the hMFB, high-frequency synapses tend to have a lower $\kappa_{E,\text{fix}}$ [43].
890 Thus, while there is a considerable heterogeneity of the functional parameters among
891 high-frequency synapses (here, the cMFB-GC and the calyx of Held synapse), some
892 parameters seem to tune synapses for high-frequency transmission. Yet, there is a
893 surprising uncertainty in many of these fundamental parameters. In particular, the
894 estimates often critically depend on the used technique (e.g. RRP_{AP} vs. $\text{RRP}_{\text{Depol}}$),
895 recording temperature (e.g., ref. [110]), and possibly also the exact species (e.g., ref.
896 [111]).
897

Table I. Properties of high- and low-frequency excitatory synapses

Property	Unit	cMFB	Calyx of Held	Boutons of neocortical pyramidal cells	Hippocampal MFB	Boutons of Schaffer collateral
Maximum instantaneous firing frequency <i>in vivo</i>	Hz	<1200 [22, 23, 92]	<800 [19]	<100 (L2/3 barrel) [109] <350 (L5B) [109] <800 (L2/3 visual) [14]	<150 [112]	<100 [113]
Presynaptic recordings established (brain slice/ <i>in vivo</i>)		yes/yes [22, 45]	yes/no [114]	no/no ^a	yes/no [115]	no/no ^b
Connectivity per synapse		1:12–1:50 [38, 116]	1:1 [117]	1:1 [118]	1:1 [31]	1:1 [119]
No. of AZs		150–300 [32, 33, 116]	600 [120]	1 [118, 121]	25 [31]	1 [119]
Diameter of AZs	nm	~150 [74, 86]	~300 [120]	~250 [111]	~300 [120]	~200 [119, 122]
AP half-width	μs	110 [11]	~100 predicted [123]	270 [124] ^c	380 [115]	n.d.
Metabolic efficiency of AP		1.8 [11]	no Na ⁺ current [125]	2 [10]	1.3 [8]	n.d.
Release probability per vesicle		0.4–0.6 [68, 69, 126] ^d	0.05–0.2 [127, 128]	0.1–0.9 [118, 121]	<0.1 [65, 129]	0.1–0.6 [119, 130, 131] ^e
Ca ²⁺ channel to vesicle coupling distance	nm	~20 [43]	~20 [62, 63] ^f	n.d. ^g	~75 [65]	30–300 [132, 133]
RRP _{AP} per AZ		1 [11, 68, 69, 126] ^h	3 [71]	2–10 [111, 134]	2 [65] ⁱ	4 [133]
RRP _{Depol} per AZ		3 [11] ^j	3–6 [71]	n.d.	30 [135]	n.d.
Replenishment rate constant	s ⁻¹	30–80 [11, 68, 69]	3–11 [136, 137] ^k	n.d.	n.d.	0.8 [138]
Exocytosis efficiency	fF pC ⁻¹	65 [42]	45 [139]	n.d.	20 [42]	n.d.
Ca ²⁺ current density	pA pF ⁻¹	145 [42]	70 [139, 140]	n.d.	70 [141]	500 [142]
AP residual [Ca ²⁺] amplitude	nM	220 [43]	500 [55]	n.d.	1,000 [56]	n.d.
AP residual [Ca ²⁺] τ decay	ms	25 [43]	45 [55]	55 [57]	45 [56]	n.d.
Ca ²⁺ -binding ratio (κ _E) of fixed buffer		15 [43]	45 [55]	140 [57]	20 [56]	n.d.
Ca ²⁺ -binding ratio (κ _E) of mobile buffer		~500 (±100 μM EGTA) [43]	~500 (±100 μM EGTA) [58]	n.d.	~1500 (±300 μM BAPTA) [65]	~250 (±50 μM Calbindin) [143] ^l

901 Abbreviations: AZ – active zone; hMFB – hippocampal mossy fiber bouton; FRP – fast releasing
902 vesicle pool; SRP – slow releasing vesicle pool; n.d. – not determined.

903

904 ^a But see refs. [124, 144] for recordings from axon initial segment and axon ‘blebs’ of L5 pyramidal
905 neurons, and ref. [145] for recordings from neocortical synaptosomes.

906 ^b But see ref. [142] for recordings from boutons of cultured hippocampal neurons and [146] for cell-
907 attached recordings in hippocampal slice cultures.

908 ^c But a duration of 150 μ s was also reported at the soma of neocortical pyramidal cells [14].

909 ^d Note that in lobule X, some mossy fibers have vesicular release probabilities ranging from 0.2–0.8
910 [147].

911 ^e The release probability of CA3 to CA3 synaptic connections is \sim 0.4 [148].

912 ^f Note that in contrast a recent study predicted an ‘exclusion zone’ separating vesicles and Ca^{2+}
913 channels by at least 30 nm [149].

914 ^g Differential EGTA-sensitivity of synapses by layer 2/3 pyramidal cells onto two types of interneurons
915 indicates target cell-specific difference of the coupling distance [66], but the high EGTA-sensitivity of
916 release indicates large coupling distances in some excitatory neocortical neurons [66, 67].

917 ^h Note that this value is not well constrained, because the binominal N per cMFB-GC connection
918 varies from 3–12 [68, 69, 126], the number of AZs per cMFB from 150–300 [32, 33, 116], and the
919 number of GCs per cMFB from 12–50 [38, 116]. The mean across all these studies is: (N per
920 connection)/((AZs per cMFB)/(GCs per cMFB)) = $7/(225/30) \approx 1$.

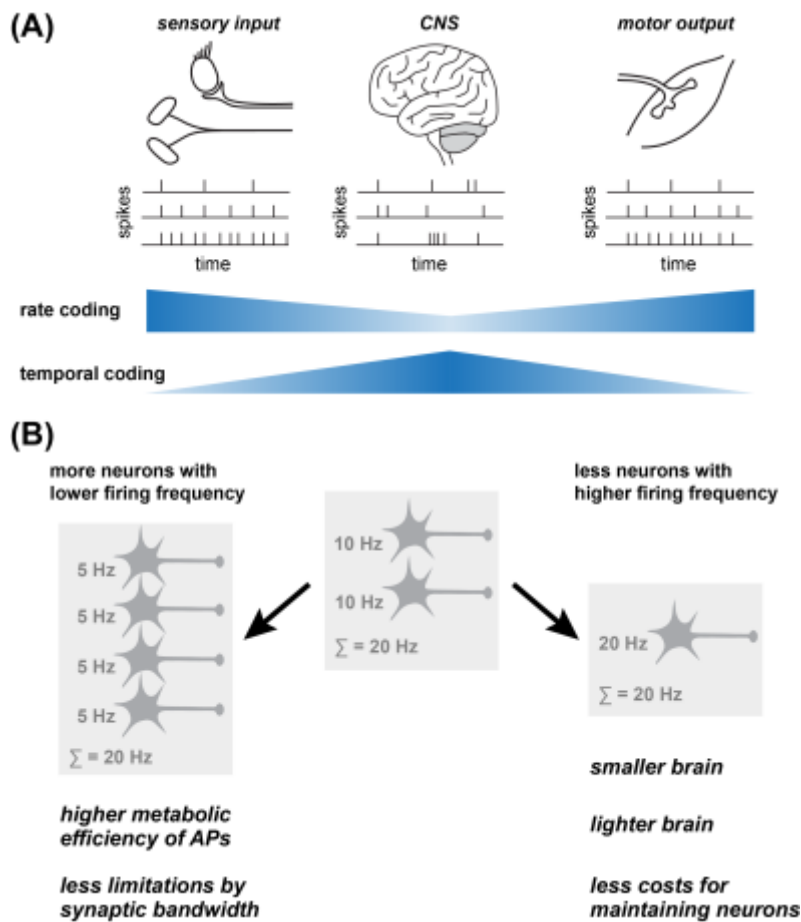
921 ⁱ Based on RRP of 53 (ref. [65]) and 25 AZ/hMFB [31]. Note that smaller estimates of RRP were
922 obtained, ranging from 7 to 16 with 1.2 and 2.5 mM extracellular $[\text{Ca}^{2+}]$, respectively, which would
923 result in an RRP/AZ < 1 .

924 ^j Based on 15 fast and 7 slow releasable vesicles and the above mentioned values of AZs and GC
925 connections, i.e. $(15+7)/(225/30) = 3$.

926 ^k Note that a rapid replenishment of fast releasing vesicles (FRP) from a pool of slowly releasing
927 vesicles (SRP) was recently described (SDR, SRP-dependent recovery; ref. [150]), which has a rate
928 constant in the range of 15 s^{-1} (E. Neher, personal communication).

929

930 **Figures and figure legends**



931

932 **Figure 1: Evolutionary constraints for high-frequency rate coding**

933 **(A)** Rate and temporal coding in the CNS and the input and output pathways.

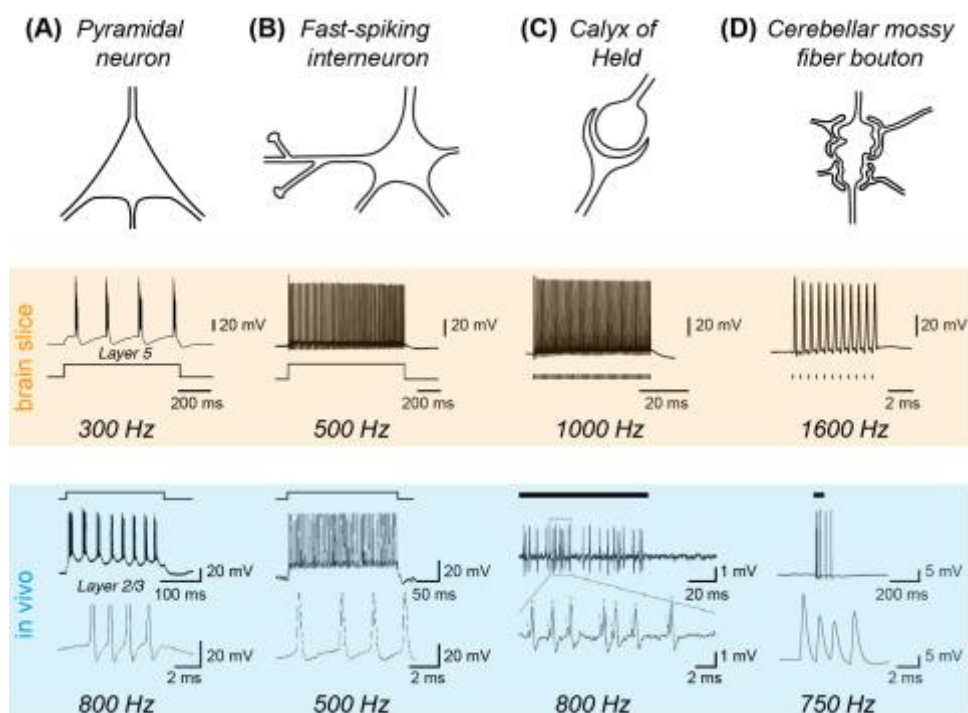
934 Whereas sensory information and motor commands are predominantly encoded via
 935 rate coding, temporal- and sparse coding becomes increasingly important in the

936 CNS. **(B)** Illustration of three cell ensembles with different number of neurons and

937 different respective average firing frequency. *Below:* Potential evolutionary

938 advantages of the corresponding cell ensembles.

939

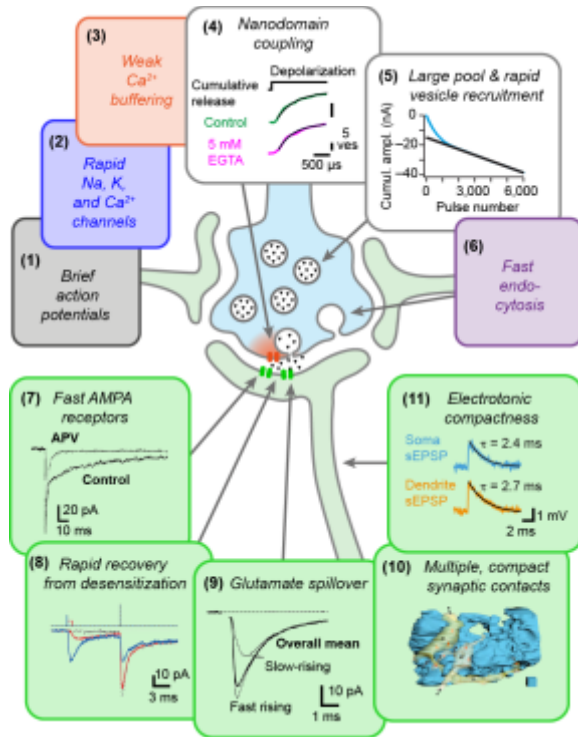


940

941 **Figure 2. Evidence for high-frequency signaling in the mammalian CNS**

942 Examples of recordings from high-frequency neurons and synapses in brain slices
 943 and *in vivo* with maximum instantaneous firing frequencies indicated (defined as the
 944 inverse of the shortest interval between APs). **(A)** Pyramidal neurons in the cerebral
 945 cortex can show typical burst firing, reaching several hundreds of Hertz within these
 946 bursts. Upper recording courtesy of M.H.P. Kole (data from ref. [108]), *in vivo*
 947 recording modified from ref. [14]. **(B)** Fast-spiking interneurons in the hippocampus or
 948 cerebral cortex display high AP frequencies with up to ~500 Hz. Upper recording
 949 modified from ref. [50], lower trace modified from ref. [16]. **(C)** The calyx of Held
 950 synapse conveying auditory information can reach Kilohertz frequencies. Upper
 951 recording modified from ref. [18], lower trace modified from ref. [19]. **(D)** Cerebellar
 952 mossy fibers and the presynaptic boutons may reach even higher AP frequencies.
 953 Upper recording modified from ref. [11], lower trace modified from ref. [22]. In brain
 954 slice recordings (orange shading), APs were elicited by current injection or axonal
 955 stimulation (indicated below the voltage traces). For the *in vivo* recordings (blue

956 shading), the stimulation is indicated above the voltage traces (current injection in A
 957 and B, tone in C, and air puff in D).
 958

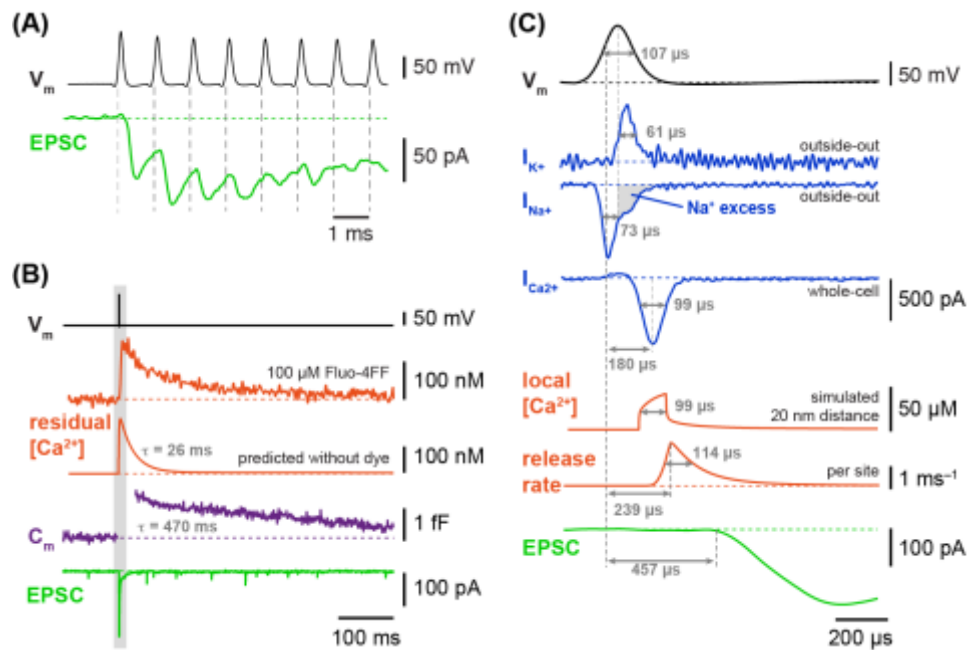


959

960 **Figure 3. Mechanisms of high-frequency synaptic transmission**

961 Summary of presynaptic (upper) and postsynaptic (lower) mechanisms supporting
 962 high-frequency synaptic transmission at the cMFB-GC synapse. The color code
 963 refers to corresponding traces in Figure 4. Data of panels 4, 5, and 7–11 are modified
 964 from refs. [42], [68], [34], [84], [85], [37], and [35], respectively.

965



966

967 **Figure 4. Rapid time course of synaptic transmission at the cMFB-GC synapse**

968 **(A)** Paired recording from a cMFB (black) and GC (green) demonstrating reliable

969 synaptic transmission at a frequency of 1 kHz (modified from ref. [11]). **(B)**

970 Comparison of the time course of presynaptic AP (black, note consistent color-code

971 in panel B and C), residual Ca^{2+} concentration (orange, *top*: measured with indicated

972 Ca^{2+} indicator, *below*: simulated without Ca^{2+} indicator dye), endocytosis (purple),

973 and EPSC (green). **(C)** Pre- and postsynaptic events on an expanded time scale.

974 The very brief presynaptic AP (black) is mediated by fast K^+ - and Na^+ -currents (blue,

975 upper), and evokes a rapid Ca^{2+} -current (blue, lower). The estimated local Ca^{2+}

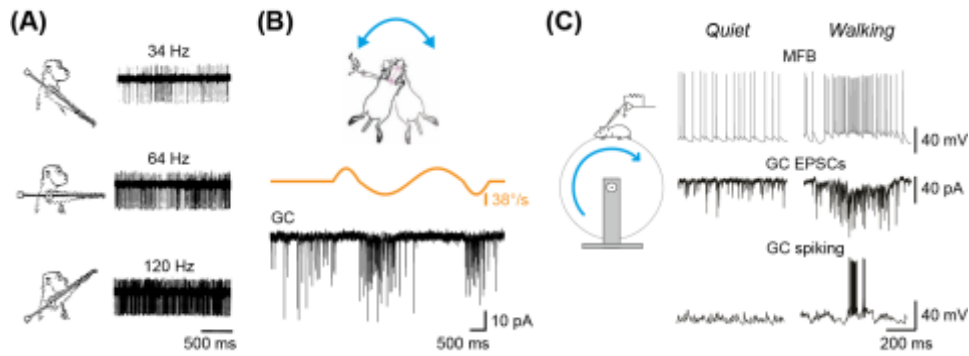
976 concentration and the release rate are illustrated in orange. The synchronous release

977 of synaptic vesicles leads to an EPSC in the postsynaptic cell (green). Delays and

978 half-widths are indicated; data are modified from refs. [11, 42, 43] and were aligned

979 to the steepest rise of the presynaptic AP.

980



981

982 **Figure 5. High-frequency coding at the cMFB-GC synapse in vivo**

983 **(A)** Extracellular recordings from awake monkeys show that a joint angle is
 984 represented in the average firing frequency of mossy fibers. Modified from ref. [91].

985 **(B)** *In vivo* recording from anesthetized mice during horizontal rotation. Rotational
 986 velocity (orange) and recording of EPSCs in granule cells (black), indicating that
 987 mossy fibers linearly encode sensory information. Modified from ref. [93]. **(C)** Pre-

988 and postsynaptic recordings from mice during locomotion. During walking, the firing
 989 frequency of mossy fibers increases (upper), leading to more EPSCs in granule cells
 990 (middle). The increased synaptic input from mossy fibers causes granule cell spiking
 991 during locomotion (lower). Modified from ref. [45].

992